PROCEEDINGS, 49th Workshop on Geothermal Reservoir Engineering
Stanford University, Stanford, California, February 12-14, 2024
SGP-TR-227

Optimizing and Monitoring Thermal Shock Stimulation of Tight Lithologies: Exploring the Impact of Repeated Thermal Shock Cycles on Timelapse Permeability and Acoustic Wave Velocities

Margariete G. Malenda and Tiziana Vanorio

Ruth Wattis Mitchell Earth Sciences Building, 397 Panama Mall, 3rd Floor, Stanford, CA, 94305

malenda@stanford.edu

Keywords: thermal shock stimulation, tight lithologies, acoustic wave velocities, permeability, enhanced geothermal systems

ABSTRACT

Immense potential for providing clean, sustainable energy through geothermal lies in producing heat through enhanced geothermal systems (EGS) in reservoirs existing several kilometers deep in the subsurface. However, to reach this potential, we must overcome two challenges. The first challenge is that EGS reservoirs are often dominated by tight (low porosity, Φ, and low permeability, *k*) crystalline rocks which require stimulation to increase *k*. While hydraulic fracturing is currently the primary stimulation method, there is great interest in developing complementary stimulation practices that could enhance the safety of stimulation. 'Thermal shocking' is one innovative stimulation method which would involve cyclically injecting surface water at pressures lower than those used in hydraulic fracturing. The surface water is relatively cooler than hot reservoir rocks, and a thermal gradient is created as the water reaches the hot rocks' mineral crystals. The crystals undergo a sudden thermal change, contract, or expand in response to induced thermal stresses, and generate thermal cracks that serve as fluid flow channels. Injection is often paused allowing the reservoir to reheat, and additional thermal cracking is induced with more injections or 'cycles'. Because this is a relatively new technique, little is known of how to optimize the effectiveness of thermal shock stimulation to reduce the amount of resources used and increase the sustainability of this practice. Here, we present time-lapse *k* measurements taken under reservoir conditions to investigate whether the number of thermal shock cycles can be optimized for increasing flow in three unique, tight lithologies relevant to EGS: granodiorite, carbonate, and basalt.

The second challenge in developing EGS is that reservoir operators must remotely monitor subsurface processes, often using geophysical methods like mapping changes in acoustic (seismic) P- and S-wave velocities (Vp and Vs respectively). Although *k* enhancing microcracks create more productive reservoirs, they are very difficult to map with measurements like seismic wave velocities. This is because we are far from understanding mechanisms behind velocity changes in tight rocks containing pore spaces that exist as subtle, thin, microcracks. Furthermore, little is known about how to optimize repeated thermal shocking using seismic data interpretations. In this work, we use time-lapse Vp and Vs measurements, taken under reservoir conditions, to assess the impact of multiple cycles on the three tight lithologies of interest and provide velocity signatures of thermally-shocked reservoir. Our measurements will inform under which reservoir conditions seismic is useful for detecting the influence of multiple cycles.

In previous studies, our time-lapse *k*, Vp and Vs measurements have been conducted on all three lithologies given a single stimulation cycle. We found that for a single cycle, lithology greatly dictated the extent of *k* increase. We also found that thermal cracking could be detected through a reduction in Vp and Vs at low effective pressure (P_{eff}). We conducted time-lapse *k* measurements of the granodiorite, carbonate, and basalt after several thermal shock cycles. Granodiorite shows modest increases in *k* with two or more cycles. Carbonate shows modest increases with three or more cycles. Basalt *k* is relatively unimpacted with up to six thermal shock cycles. We also present Vp and Vs measurements of carbonate after three cycles, showing dramatic decreases in velocities regardless of effective pressure. Ultimately, our experiments will contribute to a dataset which will help guide best practices for optimizing safe, sustainable EGS reservoir stimulation with thermal shocking.

1. INTRODUCTION

Currently, geothermal power contributes less than one percent to US electricity production (US Energy Administration system, 2023). This energy is primarily sourced from conventional geothermal systems where heat, fluid, and high values of permeability (*k*) naturally exist in a reservoir (Hamm et al., 2019). These reservoirs are often comprised of porous media, such as sandstones, which contain equant pore spaces (Hong-Bing et al., 2013). However, geothermal resources have the potential to overhaul our energy system and contribute up to 50% of the US power generating capacity (Williams et al., 2008). In order to reach this potential, reservoir operators must drill deeper to source larger amounts of heat (Hamm et al., 2019). While the exact depth varies from reservoir to reservoir, economically viable energy production is typically sought out at or deeper than 3 km (Tester et al., 2006). In these deeper systems, operators often deal with basement rocks comprised of tightly mated mineral crystals. These rocks have extremely low *k* and are called, 'tight rocks': rocks characterized by *k* below 100 μD (Law et al., 1993). Therefore, what we gain in terms of heat in deep reservoirs, we give up in terms of *k*.

In order to develop deep geothermal reservoirs, operators must overcome two challenges. First, they must increase the *k* of tight rocks to inject fluid, allow that fluid to heat up, and produce either the resultant steam or hot water. Geothermal reservoirs which require stimulation to increase *k* are called, "enhanced geothermal systems" (EGS). Hydraulic fracturing is the primary technique used to increase *k* in EGS (Huenges, 2011). However, hydraulic fracturing has been associated with induced seismicity (Ellsworth, 2013; Deichmann and Giardini,

2009; Hamm et al., 2019). Complementary stimulation methods are being investigated to reduce associated risks, (Huenges et al., 2018). Once method gaining attention is thermal shock stimulation (or 'thermal shocking'). During thermal shocking, fluid is injected from the surface into a reservoir. However, rather than relying on the increase in pore pressure or high shear stresses to create fractures, operators would rely on the thermal gradient to induce a response of mineral grains. These grains may expand or contract and then cause thermal cracks. With repeated injections (or thermal shock 'cycles'), these cracks could facilitate pathways effective enough for fluid to transport from injection to production wells (Figure 1). Additionally, these cracks could increase surface area of the reservoir and promote heat exchange between the rock and fluid (Watanabe et al., 2019).

The second challenge is that reservoir engineers must remotely monitor changes in the subsurface upon stimulation (Huenges, 2011). Geophysical tools such as seismic waves are commonly used in geothermal reservoir monitoring (Hamm et al., 2019; Tester et al., 2006). In order to detect the effectiveness of thermal shock stimulation with seismic waves, engineers must be able to interpret cracks from wave properties like compressional wave velocity (Vp) and shear wave velocities (Vs). However, correlating microstructural properties in tight rocks is much more difficult than in granular media. This is because the primary pore space in tight rocks are thin cracks, which scatter waveforms. The result is large, seemingly random scattering of Vp or Vs data.

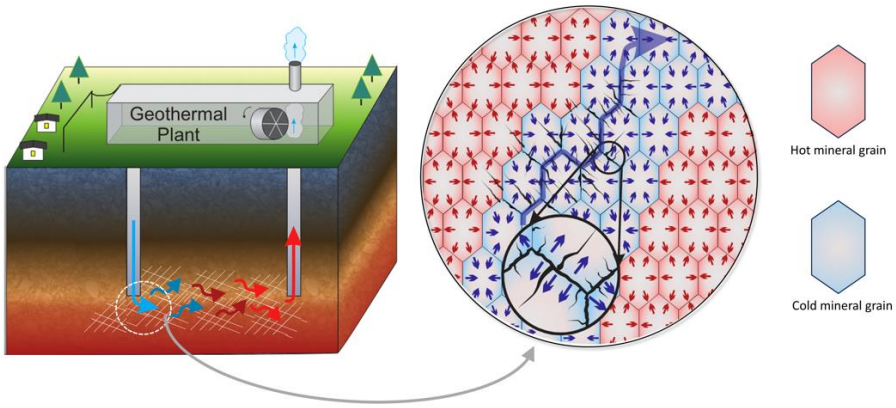

Figure 1: Schematic of thermal shocking in a geothermal reservoir. The inset shows hot mineral crystals being cooled off by injected water. Upon cooling, these minerals contract and form thermal cracks, which provide channels for fluid flow.

Because reservoir stimulation requires precious resources like water, operators must optimize the effectiveness of each injection. Previously, in Malenda and Vanorio (2023a and b), we showed that the extent of thermal cracking and evolution of *k*, Vp and Vs upon a single thermal shock cycle can be influenced by the microstructures of different tight lithologies. We tested the impact of a single thermal shock cycle on a granodiorite, basalt, and carbonate. All three lithologies have tight microstructures, low porosities, low *k*, and yet are microstructurally unique. In characterizing the microstructures, we considered the thermal conductivity, thermal expansion coefficient, and thermal anisotropy of minerals composing our samples. Such thermal properties of the minerals dictate how a bulk rock responds to a thermal gradient. In particular, we found that the granodiorite and carbonate lithologies exhibited thermal cracking with one thermal shock cycle. Basalt showed little to no thermal cracking. Our results suggest that tight rocks which have a heterogenous response of their mineral crystals to a thermal gradient will likely have greater thermal cracking than tight rocks with more homogenous responses.

Our previous work addressed the impact of one thermal shock cycle alone. In reality, reservoir engineers would require repeated stimulations in a cyclic manner (Hofmann et al., 2018). Repeated cycling could potentially increase *k* in lithologies like basalt, which resist thermal cracking upon a single thermal shock cycle. However, repeated cycling would also further exasperate the need to optimize the effectiveness of thermal shock stimulation. Therefore, we are expanding upon this work to investigate whether and how thermal stimulation can be optimized – in terms of the number of thermal shock cycles – for granites, basalts, and carbonates. We address the following question: how many cycles are needed to increase permeability for a given lithology? We also investigate the impact of thermal shock cycles on confined pressure Vp and Vs.

2. METHODS

2.1 Sample selection, mineralogical characterization, and microimaging

We've selected three tight lithologies which are prevalent in geothermal reservoirs: granodiorite, basalt, and carbonate. Specifically, we chose a Sierra White Granodiorite (SWG) from the USA, a Mt. Etna basalt (1132b) from Italy, and a Monte San Angelo carbonate (MSA) also from Italy. One sample from each lithology was curated, totaling three samples for this study. All samples are 1" diameter, 1" long cores with porosities of less than 10%. To characterize each sample's mineralogy, we used a Rigaku MiniFlex 600 Benchtop X-ray Diffraction (XRD) System. XRD results show the granodiorite is characterized by 35% calcium plagioclase, 30% sodium plagioclase, 24% quartz, 7% mica, and 4% hornblende (Figure 2). The basalt is comprised of mostly (73%) sodium plagioclase, sanidine (18%), some augite (8%), and minimal olivine and magnetite. The carbonate sample is dominated by calcite (99%), and minimal quartz (~1%). A JEOL JSM-IT500HR environmental SEM was used for microstructural imaging before and after thermal cycles. Before each imaging session, samples were coated with 15 nm of carbon using a Leica EM ACE600 coating system to prevent surface charging.

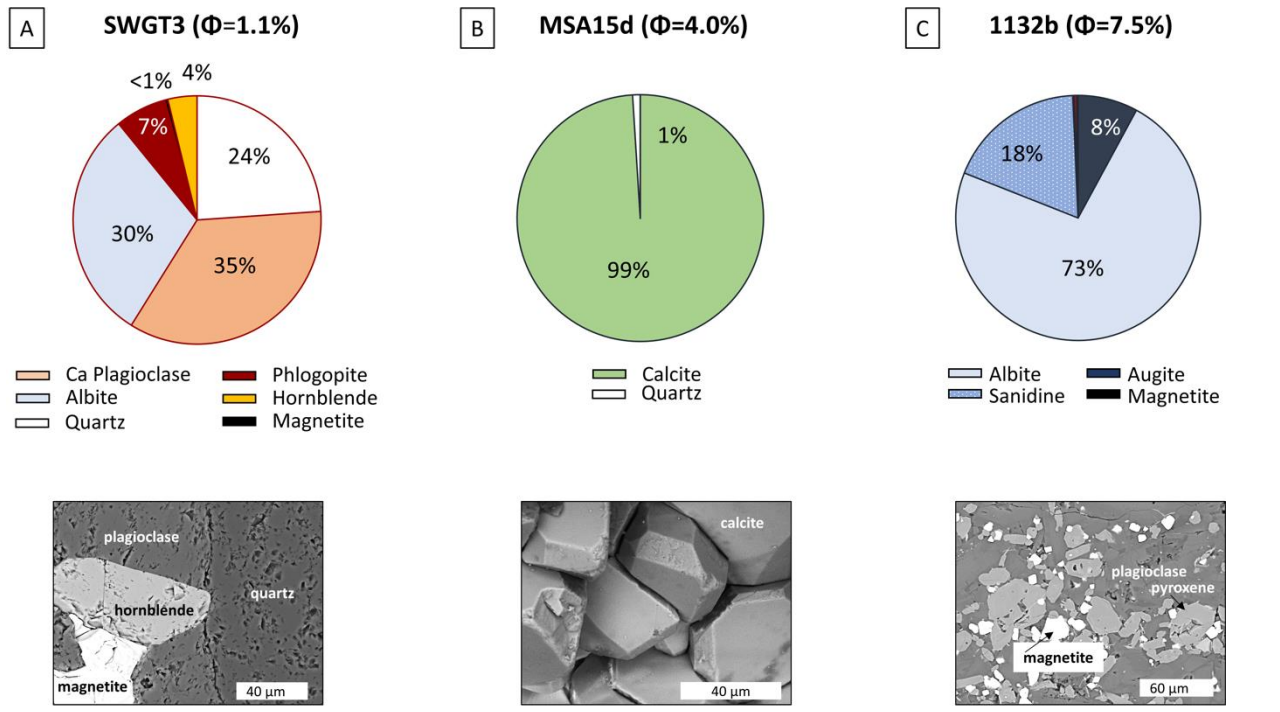

Figure 2: Initial characterization of the granodiorite (A), carbonate (B), and basalt (C) samples. Porosity for the granodiorite, carbonate, and basalt are 1.1%, 4.0 %, and 7.5%, respectively. Mineral compositions characterized with the XRD are included above electron microscopy images representative of each sample's microstructure. Mineral identification in the micro-images were collected with the energy dispersive spectroscopy.

2.2 Transport and elastic properties measurements

Prior to rock physics measurements, samples were fully dried until their weights stabilized. All samples were marked to ensure they'd be loaded into instruments in the same manner for each measurement. Connected porosity measurements are made using a benchtop helium porosimeter based on Boyle's Law of Gas expansion. Subsequently, we calculated pore volumes, connected porosity, and grain densities (ρ_g). Uncertainty related to connected porosity is within one percent (Φ unit).

Permeability was measured using the pulse-decay technique (Bourbie and Walls, 1982; Jones, 1997) and the unsteady state decay technique under confining pressure. Samples with *k* greater than 5 µD were measured using the Coretest Systems, Inc. AP-608 Automated Permeameter. The AP-608 determines the effective, or liquid *k*, of samples by measuring a pressure decay rate across the length of the sample. The AP-608 has a detection limit of 0.1 µD. The initial nitrogen pore pressure was set to 1.4 MPa, and *k* measurements were taken at elevated confining pressures that resulted in effective pressures (P_{eff}) of 5, 10, 20, 35, and 50 MPa. Samples with *k*'s less than 5 µD were measured at the same P_{eff}'s using the Coretest Systems, Inc., NDP-605 NanoDarcy Permeameter. The NDP-605 has a detection limit of 10 nD and was also connected to nitrogen for our working fluid. Through the Klinkenberg Correction (Klinkenberg, 1941), we used gas *k*'s measured at pore pressures of 1.8, 2.5 and 5 MPa to find the liquid *k* for P_{eff}'s of 5, 10, 20, 35, and 50 MPa. Uncertainty related to *k* measurements is within one percent of the *k* value.

Acoustic wave velocities were measured using the pulse transmission technique (Birch, 1960) under either benchtop or confining pressure conditions. We measured Vp and Vs using a house made acoustic pressure vessel. Samples were loaded so that each end of the sample was flush with stainless-steel endcaps that house P- (1 MHz) and S- (700 kHz) wave piezoelectric (PZ) crystals. When measuring benchtop Vp and Vs, samples remained in the endcaps without being lowered and sealed into the pressure vessel. For measurements made at confined pressure conditions, samples were lowered into the vessel, and confining pressure was increased using a pneumatic pump that pushes hydraulic oil into the vessel. Pore pressure lines were open and pores were at atmospheric pressure. Sample lengths were monitored using linear potentiometers. Acoustic waveforms were digitally displayed on the oscilloscope, from which we manually selected arrival times of the wavefronts and calculated Vp and Vs at each pressure point considering changes in sample length. Time resolution for both the P and S waves is about 100 ns. Velocity error is about 1% and is mainly attributed to error in picking the first arrival. Uncertainty in the P and S wave measurements is less than 1% of the wave velocities.

2.3 Thermal cycling protocol

First, we established a target "reservoir temperature" of 350°C, up to which we would heat the samples before cooling them to 25°C. This hot temperature is representative of various geothermal reservoirs ideal for enhanced geothermal operations (Schiffman et al., 1984; Rose et al., 2006; Reinsch et al., 2017). More importantly, we saw an opportunity to contribute something that was missing in the body of literature: testing the specific thermal change of about 325°C. Crack networks were intentionally induced in the samples by slowly heating to 350°C at a controlled heating rate of +1°C min^{-1}. We kept the samples in the oven at 350°C to equilibrate for an hour and then quickly

immersed them in a room temperature (~25°C) water bath to induce the thermal shock. All steps described here – slow heating, dwelling the samples at reservoir temperature, and then bucket quenching – constitutes how we simulate a *single thermal shock cycle* in the laboratory. To test the role of the numbers of thermal cycles, we repeated this process to simulate cyclic thermal shocking. The workflow for thermal cycling and associated measurements is shown in Figure 3.

Cycle number	0	1	2	3	4	5	6
SWGT3	Φ *k* Vp*, Vs* SEM	Φ *k* Vp*, Vs* SEM	Φ *k* Vp, Vs	Φ *k* Vp, Vs SEM	X	X	Φ *k* Vp, Vs
MSA15d	Φ *k* Vp*, Vs* SEM	Φ *k* Vp*, Vs* SEM	Φ k Vp, Vs	Φ *k* Vp*, Vs* SEM			
1132b	Φ *k* Vp*, Vs* SEM	Φ *k* Vp*, Vs* SEM	Φ k Vp, Vs	Φ *k* Vp, Vs SEM	X	X	Φ *k* Vp, Vs

* Next to Vp, Vs = measurements taken under confining pressure. X = no measurements taken.

Figure 3: Workflow to test the role of the number of thermal cycles on thermal cracking and evolution of transport and elastic rock properties. The carbonate was treated with up to three cycles. The granodiorite and basalt underwent up to six cycles. For the fourth and fifth thermal cycles, no measurements were taken. Asterisks next to Vp and Vs indicate measurements were made under confining pressure.

3. RESULTS AND DISCUSSION

3.1 Thermal cracking from repeated cycles

Micro-images of all three samples at various stages of the thermal cycling process are shown in Figure 4. The top row (A1-A3) shows the granodiorite sample before any cycling, after one thermal cycle, and after three cycles. The middle row (B1-B3) and bottom row (C1-C3) show the same stages for the carbonate and basalt samples, respectively. Across the board, any changes we observed in the microstructures take the form of either thermal crack propagation, or absence thereof. We can conclude that thermal cracking the primary mechanism of microstructural changes, because measured connected porosity, and both bulk and grain densities remain constant throughout thermal shock cycling (Table 1).

Specifically, for the granodiorite, we observed newly created thermal cracks and crack widening from the first cycle to the third cycle. We note crack propagation is predominantly intergranular and appears along quartz-plagioclase boundaries. This may result in part from the fact that quartz and plagioclase have very different thermal properties and therefore different responses to a given thermal gradient.

Between the first and third thermal cycle, cracks propagated extensively throughout the carbonate. Thermal cracks which were newly formed after the first thermal cycle had been widened with subsequent cycling. Whether these cracks are intragranular or not is not yet distinguishable from our SEM images. In Malenda and Vanorio, 2023, we discussed how extensive thermal cracking in carbonate can be correlated with the fact that the microstructure is comprised of primarily calcite. Calcite has an anisotropic thermal expansion coefficient, such that when in the presence of a thermal gradient, there will be expansion along one mineral crystallographic axis and contraction along the other. In a mosaic of tightly interlocked, randomly oriented calcite mineral grains, some grains will expand in a given direction and others will contract causing stresses along grain boundaries.

For the basalt, no thermal cracking was observed with repeated cycling. This behavior is similar to what was observed upon a single thermal cycle in Malenda and Vanorio, 2023. We attribute the minimal/lack of thermal cracking to the fact that basalt is comprised of primarily plagioclase minerals. Plagioclase minerals have relatively low thermal expansion coefficient and thermal conductivity. Additionally, the spread in thermal properties of the basalts is relatively small, indicating the various mineral crystal grains will respond similarly to one another for a given thermal gradient. This similarity in response will reduce the stress build up along grain boundaries and reduce the potential for thermal cracking.

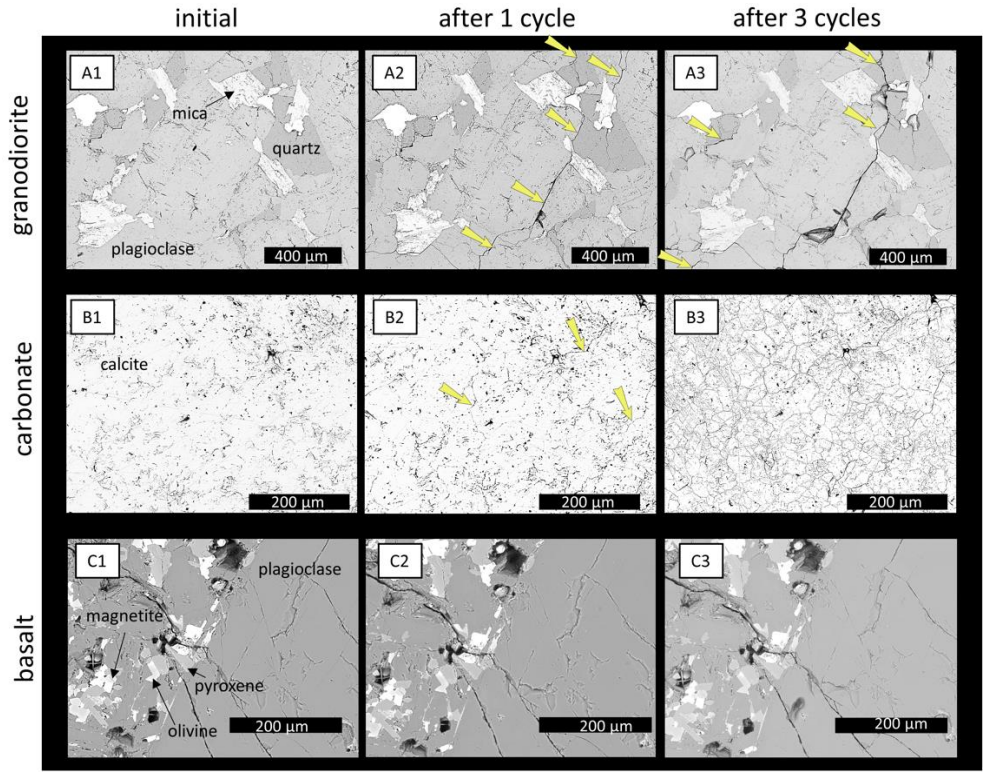

Figure 4: Microimaging of locations in the granodiorite (A1-A3), carbonate (B1-B3), and basalt (C1-C3) throughout thermal cycling. The initial microstructures are shown (A1, B1, C1) as well as the same locations after a single thermal cycle (A2, B2, C2) and after three thermal cycles (A3, B3, C3). Yellow arrows indicate presence of newly created cracks with the exception of B3. Cracking through the carbonate is so pervasive, the inclusion of arrows would only make it difficult to see the extent of cracking.

Table 1: Porosity, grain density, and bulk density measurements for the granodiorite, carbonate, and basalt samples with repeated thermal cycling.

Cycle Number	Sample	Porosity (%)	Grain Density (g cm^{-3})	Bulk Density (g cm^{-3})
0	granodiorite	1.13	2.77	2.74
1		1.15	2.77	2.74
2		1.18	2.77	2.74
3		1.24	2.77	2.74
6		1.45	2.78	2.74
0	carbonate	4.01	2.68	2.57
1		5.03	2.69	2.56
2		5.65	2.70	2.55
3		5.33	2.70	2.55
0	basalt	7.49	2.84	2.63
1		8.40	2.87	2.63
2		8.22	2.86	2.63
3		8.48	2.86	2.62

6		8.72	2.87	2.62

3.2 Optimized permeability under pressure

Permeability measurements made under confining pressures are shown in Figure 5. Prior to thermal shocking, the granodiorite's *k* was below the detection limit of our NDP (A). The greatest increase in *k* occurred upon the first thermal shock cycle, where *k* increased from less than 0.01 μD to more than 0.1 μD. However, with additional thermal cycling, *k* exhibits slight increases, even at effective pressures up to 50 MPa. Therefore, whichever cracks are being populated with the subsequent cycles, are stiff enough to withstand the pressure and continue to allow fluid to flow. This implies that while the increase in *k* is not substantial from the first to the sixth cycle, a modest increase can be expected regardless of P_{eff} conditions in the geothermal reservoir (up to 50 MPa).

Permeability in the carbonate increases up to 10 μD with the first thermal cycle and increases almost another order of magnitude with the second cycle (Figure 5b). Comparatively, permeability continues to increase with the third thermal cycle, but to a much lesser extent. One potential reason is that the stresses imposed during first and second thermal cycles were enough to create major cracks which could serve as the primary fluid flow channels. If the sample already has cracks serving as primary flow channels, these cracks can allow for surrounding mineral grains to expand or contract freely in the presence of a thermal gradient. In other words, the sample may be able to accommodate stresses that are applied with the third cycle. It is also worth noting that the slight increase upon the third cycle is present even at higher P_{eff}, similar to those of granodiorite.

For the basalt, it is clear that *k* does not increase substantially with thermal cycling (Figure 5C). In fact, there is a slight decrease in *k* with additional cycles at elevated P_{eff}. This may be explained by the idea that there are effectively two opposite and opposing processes occurring in the microstructures of all the samples which impact *k* measurements. The first process is that of thermal cracking which will ideally create and connect once isolated cracks or pore spaces to increase *k*. The second process is that with thermal cracking – including lengthening or widening of pre-existing cracks – these thin, pressure sensitive pore spaces are becoming slightly more compliant. For the granodiorite and carbonate, the first process is far outweighing the second. This is why we see continued *k* increases, even if ever so slight. For the basalt, the increase in crack compliance with repeated thermal cycles is outweighing the effect of crack propagation and crack connection. It could be that while all samples are experiencing the same increase in crack compliance, the granite and carbonate experience greater degrees of crack propagation and connection compared to the basalt. These are valuable insights for reservoir operators prospecting reservoirs with relatively higher P_{eff}. Thermal shocking will be more useful for granodiorite and carbonate reservoirs with high P_{eff}. Alternatively, this stimulation technique may backfire in basaltic reservoirs with high P_{eff}.

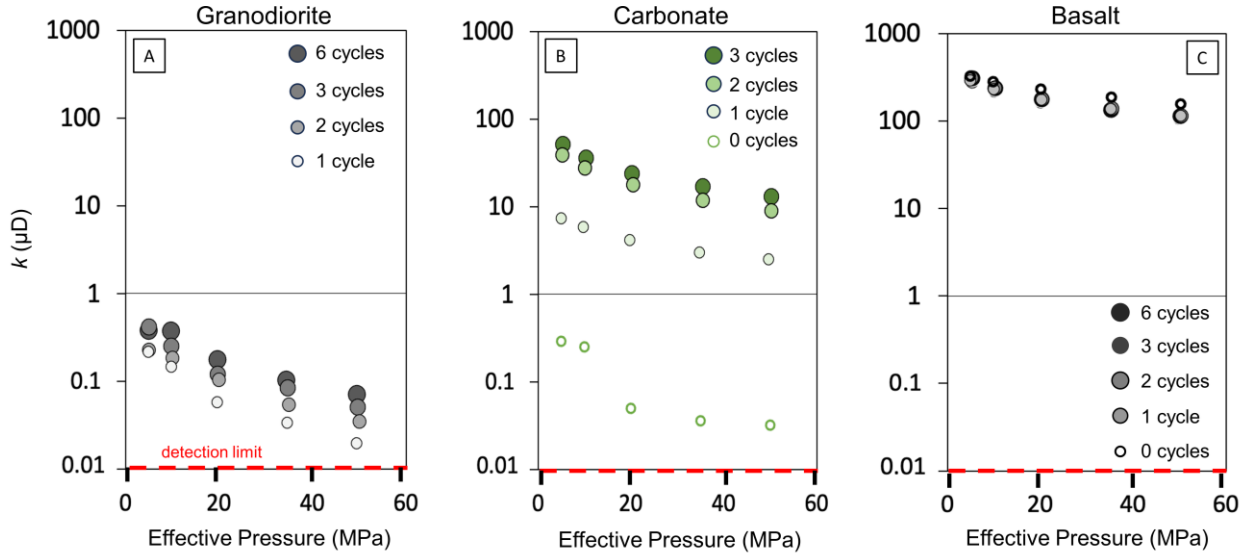

Figure 5: Permeability measurements for the granodiorite (A), carbonate (B), and basalt (C) samples upon thermal cycling. Hollow symbols indicate pre-treatment *k* measurements. In the case of granite, prior to treatment, the permeability was below the NDP detection limit. For symbols filled with color, the darker colors and larger symbols indicate measurements made after higher numbered cycles.

3.3 Thermal crack detection with acoustic wave velocities

Benchtop Vp and Vs measurements of the three lithologies are shown in Figure 6A and B, respectively. Regardless of the extent of observed cracking or increase in *k*, both Vp and Vs for all lithologies decrease with thermal cycles. In general, decreases in Vp and Vs reflect the presence of newly formed or propagating cracks that interrupt the paths of acoustic waves passing through the sample's mineral grains and scatter the wave energy (Biot, 1962; Kuster and Toksöz, 1974; Likharev, 2013; Snieder, 2002). The decrease, however, is greater for the granodiorite and carbonate compared to the basalt, reflecting the greater extent of cracking observed with SEM. Yet the

continued slight decrease in Vp and Vs in basalt does support that pre-existing cracks become more compliant in the basalt. This further substantiates the idea that basalt's *k* decreases with increased pressure due to great crack compliance.

For granodiorite, Vp decreases by about 2 km s^{-1} with up to three cycles. This result is consistent with those from Griffiths et al., (2018), who heated granite samples at 1°C min^{-1} to 450°C, and then cooled samples with a built in cooling system.

We see a gradual decrease of Vp in all samples with repeated thermal cycles. This is much more gradual than the sharp decrease in benchtop Vp (-3 km s^{-1}) that Rong et al., (2018) observed with up to only 2 cycles. After the second cycle, their Vp measurements remained relatively constant with up to 16 cycles. Rong et al., (2018) induced thermal cycling on a granite and marble sample, through heating at 10°C min^{-1} to 600°C and then cooled samples to ambient temperature by placing them on a countertop. Likely their faster heating rate and greater thermal gradient with cooling (575°C) contributes to a larger decrease in Vp after the first cycle compared to what we observe. Additionally, damage in their granitic samples may have been exasperated with the first cycle by the fact that beyond 400°C, quartz in granite undergoes a phase transition (Shang et al., 2018). During the transition, the crystallographic structure is altered which could lead to further cracking.

Kim et al., (2014) observe only a slight to no decrease in benchtop Vp for both granite and diabase upon five cycles. However, they heated their samples at 1°C min^{-1} to only 100°C. No images were included to show the presence of newly formed thermal cracks.

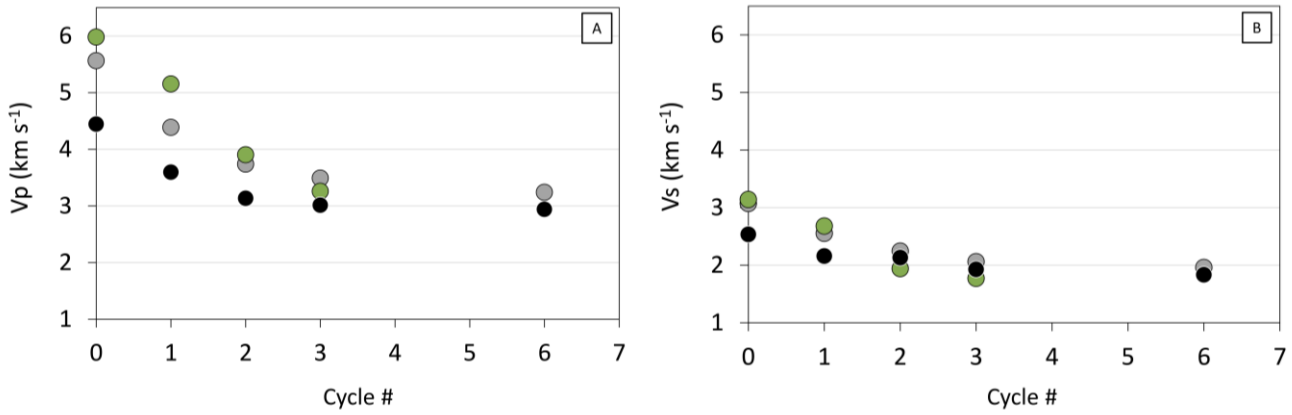

Figure 6: Benchtop Vp (A) and Vs (B) measurements for the granodiorite, carbonate, and basalt samples for up to 6 thermal cycles. Grey data is for the granodiorite, green is for the carbonate, and black is for basalt.

Figure 7 shows Vp and Vs measured under confining pressures for the carbonate sample after zero, one, and three thermal shock cycles. Both Vp and Vs decrease substantially with additional thermal cycling. From one cycle to three, Vp reduces by almost 2 km s^{-1} when P_{eff} is zero, and Vs decreases by almost 1 km s^{-1}.

The decrease is most evident at the lower P_{eff}'s but is substantial regardless of the pressure. Anselmetti and Eberle (1993) also documented decreases in confined pressure Vp and Vs in cracked carbonates. With increased confining pressure, their Vp also increased due to crack closure. Reduced Vp and Vs at higher pressures indicates that newly formed cracks are not fully closed with heightened pressure. This helps explain why even at higher P_{eff}'s, there is such a great increase in *k* for the carbonate multiple cycles. Our results show that across a range in P_{eff}'s, carbonate's *k* increased and that acoustic wave velocities decreased overall. This suggests that it could be possible to remotely monitor thermal cracks facilitating fluid flow in carbonate geothermal reservoirs, under various pressure conditions.

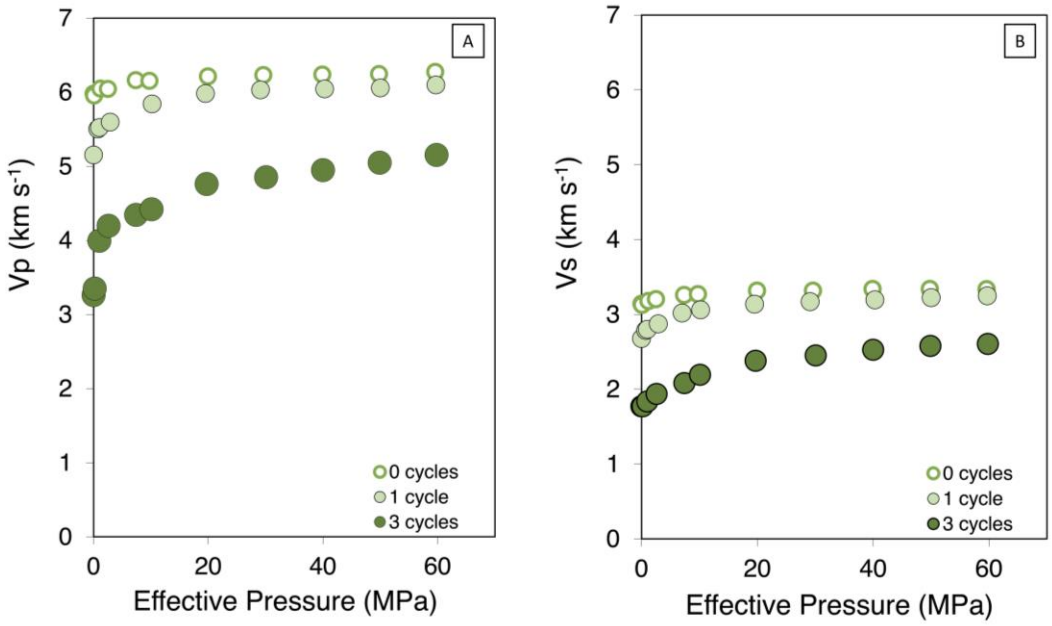

Figure 7: Vp (A) and Vs (B) measurements on the carbonate sample with up to 60 MPa before any thermal cycling, after a single thermal cycle, and after three thermal cycles.

4. CONCLUSIONS

We provide a comprehensive dataset capturing the extent of thermal cracking and resulting evolution in *k*, Vp, and Vs in carbonate, granodiorite, and basalt exposed to cyclic thermal shocking. Using observations from time-lapse microimaging, we are able to explain changes in *k*, Vp, and Vs with up to six thermal shock cycles. Lithologies with minerals characterized by a spread in thermal properties (i.e., thermal conductivity and expansion coefficient) show continued increase in *k* with repeated shocking. For example, the granodiorite shows modest, but persistent increases in *k* with up six thermal cycles. Vp and Vs measurements of the granodiorite reflect the presence of continued thermal cracking with additional cycles. The carbonate, a lithology dominated by thermally anisotropic calcite, experienced major increases in *k* with the first and second thermal cycle, but modest increases thereafter. The increases in *k* were facilitated by pervasive microcracking, which was easily observable with SEM imaging. Additionally, these microcracks created with subsequent cycles were detected even at high P_{eff}'s through large decreases in Vp and Vs between cycles. Similarly, in a lithology like basalt, the impact of thermal shocking is also detectable using Vp and Vs. However, this thermal cracking actually leads to slight decreases in *k* at higher P_{eff} due to increasing crack compliance. Thus far, we conclude that cyclic thermal shocking is most suitable for lithologies like carbonate and granodiorite, which are comprised of minerals which respond anisotropically or heterogeneously to thermal gradients. Cyclic shocking may slightly improve *k* in lithologies like granodiorite with large spreads in the thermal properties of its mineral composition. Very likely, cyclic thermal cycling will not be effective for thermally insensitive lithologies like basalt, especially at higher P_{eff}'s. We will continue our study, testing up to ten cycles on all three lithologies. After the tenth cycle, we will include a final documentation of the microstructures with SEM imaging and a final dataset of *k*, Vp, and Vs for all samples.

ACKNOWLEDGEMENTS

We would like to acknowledge the assistance of Juan Salvador Lezama Pacheco at the Stanford Environmental Measurements Facility with XRD data collection and analysis. We appreciate the technical support of Dale Burns Stanford Scanning Electron Microscope Facility. This work was supported by the Stanford Rock Physics Affiliates Program, the former Stanford School of Earth, Energy, and Environmental Sciences, and the Stanford Doerr School of Sustainability.

REFERENCES

Anselmetti, F.S. and Eberli, G.P.: Controls on Sonic Velocity in Carbonates, Pure and Applied geophysics, 141, (1993), 287-323.

Biot, M.A.: Mechanics of Deformation and Acoustic Propagation in Porous Media, Journal of Applied Physics, 33, 4, (1962), 1482-1498.

Birch, F.: The Velocity of Compressional Waves in Rocks to 10 kilobars, Journal of Geophysical Research, 65, (1960), 1083–1102.

Bourbie, T., and Walls, J.: Pulse Decay Permeability: Analytical Solution and Experimental Test, 3, (1982).

Deichmann, N. and Giardini, D.: Earthquakes Induced by the Stimulation of an Enhanced Geothermal System below Basel (Switzerland), Seismological Research Letters, 80, 5, (2009), 784-798.

Ellsworth, W.L.: Injection-Induced Earthquakes, Science, 341, 6142, (2013), 1225942.

Griffiths, L., Lengliné, O., Heap, M.J., Baud, P. and Schmittbuhl, J.: Thermal Cracking in Westerly Granite Monitored Using Direct Wave Velocity, Coda Wave Interferometry, and Acoustic Emissions, Journal of Geophysical Research: Solid Earth, 123, 3, (2018), 2246-2261.

Hamm, S., Hass, E., Winick, J., Tasca, C., Albayrak, F., and Augustine, C.: GeoVision: Harnessing the Heat Beneath our Feet, Chapter 2, What is Geothermal Energy, US Department of Energy, (2019).

Hofmann, H., Zimmermann, G., Zang, A. and Min, K.B.: Cyclic Soft Stimulation (CSS): a New Fluid Injection Protocol and Traffic Light System to Mitigate Seismic Risks of Hydraulic Stimulation Treatments, Geothermal Energy, 6, 1, (2018), 1-33.

Hong-Bing, L., Jia-Jia, Z., Feng-Chang, Y.: Inversion of Effective Pore Aspect Ratios for Porous Rocks and its Applications, Chinese Journal of Geophysics, 50, 1, (2013), 43-51.

Huenges, E., Ellis, J., Hofmann, H., Zimmermann, G., Brehme, M., Farkas, M., Westaway, R., Burnside, N., Min, K.B., Yoon, K. and Genter, A.: Concepts of Soft Stimulation Treatments in Geothermal Reservoirs, Geothermal Resources Council Transactions, 42, (2018).

Huenges, E.: Geothermal Energy Systems: Exploration, Development, and Utilization, John Wiley & Sons, (2011), 52-181.

Jones, S. C.: A Technique for Faster Pulse-Decay Permeability Measurements in Tight Rocks, Society of Petroleum Engineers Formation Evaluation, 12, (1997), 19–25.

Kim, K., Kemeny, J. and Nickerson, M.: Effect of Rapid Thermal Cooling on Mechanical Rock Properties, Rock Mechanics and Rock Engineering, 47, (2014), 2005-2019.

Klinkenberg, L.J.: The Permeability of Porous Media to Liquids and Gases: API, Drilling and Production Practice, (1941), 200–213.

Kuster, G.T. and Toksöz, M.N.: Velocity and Attenuation of Seismic Waves in Two-Phase Media: Part I. Theoretical Formulations, Geophysics, 39, 5, (1974), 587-606.

Law, B.E., and Spencer, C.W., and Howell, D.G.: Gas in tight reservoirs-an emerging major source of energy. The future of energy gases, US Geological Survey Professional Paper, 1570, (1993), 233-252.

Likharev, K.: Radiation, Scattering, Interference and Diffraction in Essential Graduate Physics: Stony Brook University, (2013).

Malenda, M. and Vanorio, T.: Using Acoustic Velocities and Microimaging to Probe Microstructural Changes Caused by Thermal Shocking of Tight Rocks, Frontiers in Earth Science, 10, (2023), 1054469.

Malenda, M. and Vanorio, T.: Using Acoustic Velocities and Microimaging to Probe Microstructural Changes caused by Thermal Shocking of Tight Rocks, Geothermal Rising, Geothermal Resources Council Transactions

Reinsch, T., Dobson, P., Asanuma, H., Huenges, E., Poletto, F. and Sanjuan, B.: Utilizing Supercritical Geothermal Systems: A Review of Past Ventures and Ongoing Research Activities, Geothermal Energy, 5, 1, (2017), 1-25.

Rong, G., Peng, J., Cai, M., Yao, M., Zhou, C. and Sha, S.: Experimental Investigation of Thermal Cycling Effect on Physical and Mechanical Properties of Bedrocks in Geothermal Fields. Applied Thermal Engineering, 141, (2018), 174-185.

Rose, P., McCulloch, J., Adams, M. and Mella, M.: An EGS Stimulation Experiment Under Low Wellhead Pressures, Proceedings, 13th Workshop on Geothermal Reservoir Engineering, Stanford University, Stanford, CA (2005).

Schiffman, P., Elders, W.A., Williams, A.E., McDowell, S.D., and Bird, D.K.: Active Metasomatism in the Cerro Prieto Geothermal System, Baja California, Mexico: a Telescoped Low-Pressure, Low-Temperature Metamorphic Facies Series, Geology, 12, 1, (1984), 12-15.

Shang, X., Zhang, Z., Xu, X., Liu, T. and Xing, Y.: Mineral Composition, Pore Structure, and Mechanical Characteristics of Pyroxene Granite Exposed to Heat Treatments, Minerals, 9, 9, (2019), 553.

Snieder, R.: General Theory of Elastic Wave Scattering *in* Scattering and Inverse Scattering in Pure and Applied Science, eds. Pike, R. and P. Sabatier, Academic Press, San Diego, (2002), 528-542.

Tester, J.W., Anderson, B.J., Batchelor, A.S., Blackwell, D.D., DiPippo, R., Drake, E.M., Garnish, J., Livesay, B., Moore, M.C., Nichols, K. and Petty, S.: Chapter 1, Synopsis and Executive Summary *in* The Future of Geothermal Energy, Massachusetts Institute of Technology, 358, (2006), 1-12.

United States Energy Information Administration: Electric Power Annual 2022, Chapter 3. Net Generation, Washington, DC (2023), 32-64.

Watanabe, N., Sakaguchi, K., Goto, R., Miura, T., Yamane, K., Ishibashi, T., Chen, Y., Komai, T. and Tsuchiya, N.: Cloud-Fracture Networks as a Means of Accessing Superhot Geothermal Energy. Scientific reports, 9, 1, (2019), 939.

Williams, C. F., Reed, M.J., Mariner, R.H., DeAngelo, J., Galanis, S.P.J.: Assessment of Moderate- and High-Temperature Geothermal Resources of the United States, U.S. Geological Survey Fact Sheet 2008-3082, U.S. Department of Interior (2008).